

Cascade-type hybrid energy cells for driving wireless sensors



Guocheng Liu^{a,*}, Nezhir Mrad^b, Eihab Abdel-Rahman^c, Dayan Ban^{a,*}

^a Department of Electrical & Computer Engineering, Waterloo Institute for Nanotechnology, University of Waterloo, Waterloo, Ontario, Canada N2L 3G1

^b Defence Research and Development Canada, Department of National Defence, National Defence Headquarters Ottawa, ON, Canada K1A 0K2

^c Department of Systems Design Engineering, Waterloo Institute for Nanotechnology, University of Waterloo, Waterloo, Ontario, Canada N2L 3G1

ARTICLE INFO

Article history:

Received 25 January 2016

Received in revised form

3 June 2016

Accepted 11 June 2016

Available online 18 June 2016

Keywords:

Nanogenerator

Solar cell

ZnO nanowire

Homojunction

Wireless sensor

ABSTRACT

This paper presents a cascade-type compact hybrid energy cell (CHEC) that is capable of individually and concurrently harvesting solar and strain energies. The cell is made up of an *n-p* homojunction nanowire (NW)-based piezoelectric nanogenerator and a nanocrystalline/amorphous-Si:H single junction cell. Under optical illumination of ~ 10 mW/cm² and mechanical vibration of 3 m/s² at 3 Hz frequency, the output current and voltage from a single 1.0 cm²-sized CHEC, 280 μ A and 3.0 V, respectively, are sufficient to drive low-power commercial electronics. Six such CHECs connected in series generate enough electrical power to light emitting diodes or drive a wireless strain gauge sensor node.

© 2016 Elsevier Ltd. All rights reserved.

1. Introduction

Solar [1–5] and vibration [6–8] energies are most commonly available in the ambient environment. They can be harvested, converted into electrical energy and used to operate autonomous wireless sensor networks (WSNs) [9]. However, vibrations generate power only while motion persists and solar energy is significant only when optical illumination is sufficient. Thus, a technology that can harvest energy from both sources would produce more reliable and substantial power output. The nanotechnology-based compact hybrid energy cell (CHEC) proposed here can individually and concurrently harvest vibrations and/or solar energies [10,11].

Various CHECs have been proposed for harvesting vibration, solar, thermal and chemical energies [10–29]. For example, functioning CHECs made of intrinsic ZnO nanowires (NWs) and organic polymer blends have been reported to harvest strain and solar energies [10–15]. Semiconductor NWs exhibit unique features for energy harvesting applications, such as enhanced surface area, high mechanical flexibility, high sensitivity to small forces, better charge collection, enhanced solar energy absorption through light trapping, and amenability to function as a template for other structures [2,3]. On the other hand, the increased surface area in high aspect-ratio NW structures may also cause greater non-radiative recombination across local junctions/interfaces due to

surface defects, which often undercuts these advantages [30–32].

In typical hybrid energy harvesters, the components that scavenge different types of energy are designed and fabricated independently, following distinct physical principles. Due to their different output characteristics, each energy harvesting modality requires its own power conversion and management circuitry. For example, piezoelectric nanogenerators (NGs) have large output impedance and can produce high voltage but low current, while solar cells (SCs) have small output impedance, with high current but low voltage [14]. Designing compact cells that can effectively and simultaneously harvest energy from multiple types of sources will increase their applicability and levels of output power. Complementary harvesting can also be used to improve the output characteristics by increasing output current and voltage simultaneously. Achieving these goals requires innovative and integrated methods, materials, and structures [10,11].

Herein, we present the first cascade-type transparent vibration/solar energy cell synthesized on a polyethylene naphthalate (PEN) flexible substrate. The cascade-type CHEC's monolithically-integrated two-terminal structure substantially suppresses the large interfacial electrical losses typically encountered in mechanically stacked devices. Furthermore, integrating the solar cell on top of the piezoelectric nanogenerator significantly enhances output power density, through effective, simultaneous and complementary harvesting of ambient strain and solar energies. The cell consists of a vertically-aligned *n-p* ZnO homojunction NW-based nanogenerator and a hydrogenated nanocrystalline/amorphous silicon (nc/a-Si:H) *n⁺-i-p⁺* junction solar cell. The device's

* Corresponding authors.

E-mail addresses: g37liu@uwaterloo.ca (G. Liu), dban@uwaterloo.ca (D. Ban).

full inorganic heterostructure improves chemical stability and mechanical durability. It can function as a sensor, a solar cell, or a nanogenerator.

2. Materials and methods

2.1. ZnO *n-p* homojunction NW growth

The ZnO homojunction NWs are grown hydrothermally [33]. A SiN buffer layer and aluminum-doped ZnO (AZO, 2 wt% Al₂O₃ + 98 wt% ZnO) layer are deposited onto a pre-cleaned polyethylene naphthalate (PEN) substrate using radio-frequency (RF) magnetron sputtering at 150 °C. The SiN buffer layer improves the surface properties of the substrate. The AZO layer serves as a conductive electrode as well as a seed layer for subsequent ZnO NW growth. The aqueous solution for growing *n*-type ZnO NWs is a mixture of zinc (Zn) nitrate hexahydrate (25 mM), hexamethylenetetramine (25 mM) and aluminum (Al) nitrate nonahydrate. The atomic ratio of Al to (Al+Zn) in the mixture solution is controlled at 3 wt%. To obtain *p*-type ZnO NWs, a doping reagent, lithium (Li) nitrate (75 mM), is added to the solution (heavily *p*-type). The solution is kept at a constant temperature of 88 °C during growth, and the ZnO NW length is simply controlled by growth time (~500 nm/h): one hour for the *n*-type section immediately followed by an additional half hour for the Li-doped *p*-type section. Additionally, the *n-n* homojunction NWs are prepared with intrinsic (effectively *n*-type) NW growth procedure for use as control samples in the experiments [33]. All samples are cleaned using a standard process.

2.2. Fabrication of the compact hybrid energy cell

The solar component of the CHECs consists of a stack of *n⁺-i-p⁺* nc/a-Si:H thin-film layers, deposited on top of the synthesized *n-p* and *n-n* homojunction ZnO NWs by plasma-enhanced chemical-vapor deposition (PECVD) at a substrate growth temperature of 150 °C. A 13.56 MHz PECVD cluster system is first used to deposit 60 nm of *n⁺* nanocrystalline (nc)-Si:H thin-film onto the NW array at an RF power density of 194 mW/cm², using a combination of SiH₄/H₂/pH₃ gases. Immediately after, a 500 nm thick *i-a-Si:H* intrinsic absorber layer is deposited at a power density of 9 mW/cm² by flowing SiH₄, followed by 60 nm of *p⁺* nanocrystalline (nc)-Si:H deposited at a power density of 43 mW/cm² using SiH₄/H₂/B₂H₆ process gases. Lastly, a 200 nm thick AZO layer is deposited as a transparent front contact. Photolithography is then employed to pattern the stack into arrays of square CHECs. Silver conductive paste is used to glue Cu wire leads onto the top and bottom AZO electrodes. The completed stacks are packaged in polydimethylsiloxane (PDMS), Dow Corning Sylgard 184, pre-mixed with curing agent at a ratio of 10:1 w/w, and then degassed to prevent contamination, damage, and moisture penetration from the ambient environment.

2.3. Structural and device characterization

The morphology of the as-grown ZnO NWs is obtained using a Zeiss Orion Plus helium ion microscope (HIM). Optical characterization of the NW structures is performed using a UV/Visible spectrophotometer (Shimadzu, UV-2501PC). The ZnO nanowires in the CHECs were grown following methods validated in a previous study [34] and shown to successfully incorporate Li ions into the ZnO lattice, resulting in *p*-type doped nanowires. The current-voltage (*I-V*) curves of the CHECs and their junction capacitance are measured using a Keithley 4200-SCS semiconductor characterization system, calibrated before measurement to keep the system noise at or below 1fF in a wide frequency range (1 kHz–

10 MHz). The photovoltaic parameters are measured under 1-sun AM 1.5G radiation from an ABET Sun 3000 Class AAA solar simulator with a Keithley 2400 source/meter. Piezoelectric characterization is carried out using a system that includes a closed-loop controller (Vibration Research Corporation, VR9500) and a linear shaker (Labworks Inc., ET-126B-1) to provide sinusoidal waves simulating a vibration source with a known amplitude and frequency. Output piezoelectric voltage and current signals are measured using low-noise voltage/current preamplifiers (Stanford Research System Model SR560/570) and a National Instruments I/O module (NI CompactDAQ USB-9239). The input resistances of the voltage and current preamplifiers are 100 MΩ (SR560) and 10 kΩ (SR570), respectively. To minimize electromagnetic interference, the two copper wires connected to the device under test are twisted together. All measurements are conducted at ambient room temperature.

3. Results and discussion

Fig. 1a shows a schematic diagram of a fabricated CHEC and its architecture. An equivalent circuit of the CHEC, showing the NG and SC connected in series, appears in Fig. 1b. The nc/a-Si:H *n⁺-i-p⁺* layers are integrated directly on top of the underlying lithium-doped ZnO nanowire layer. Two types of ZnO NWs are employed in the device fabrication: ZnO *n-p* homojunction NWs and ZnO *n-n* homojunction NWs. Fig. 1c shows a photograph of the patterned array of CHECs with varying side lengths (from 1 mm to 1 cm) and insulation separation. This array configuration provides the basis for effectively comparing the output for a range of CHECs. Fig. 1d shows a cross-sectional helium ion microscope (HIM) image of a typical CHEC, and confirms the monolithic and seamless integration between the nc/a-Si:H *n⁺-i-p⁺* layers and the underlying ZnO NW layer. The ZnO NWs are functioning as the piezoelectric material for mechanical energy conversion and as the electron transport layer for photocurrent collection of the solar cell component. Fig. 1e shows top-view HIM images of the as-grown *n-p* and *n-n* homojunction ZnO NWs, revealing uniform growth of high-density and vertically-aligned NWs. The average length and diameter of these NWs are ~750 nm and 80 nm, respectively.

This monolithic CHEC can exploit piezopotential under compressive strain and photovoltaic potential under ambient optical illumination, to generate electrical power. The CHECs, when placed solely under optical illumination, function as traditional solar cells and produce continuous photocurrent output. The photocurrent flows from the *n⁺*-nc-Si layer to the *p⁺*-nc-Si layer, or from the left (the bottom) to the right (the top), as illustrated in Fig. 1a. When a compressive force is applied, negative piezopotential (V_-) is generated at the AZO/*n*-ZnO NW interface (bottom) and positive piezopotential (V_+) at the *p*-ZnO NW/*n⁺*-nc-Si interface (the top). The photovoltaic potential and the piezopotential are in the same direction and thus are added together [11]. The combined potential creates a stronger voltage drop between the positive (top) port and the negative (bottom) port, which drives current through an external load. Owing to the high interfacial energy barrier, electrons accumulate at the interface between the *p⁺*-nc-Si layer and top AZO electrode until the resulting potential balances the piezopotential in an equilibrium state. Once the compressive load is released, the piezopotential drops to zero, and the electrons accumulated around the *p⁺*-nc-Si layer flow back to the bottom AZO electrode via the external circuit. Consequently, a negative electric pulse is generated and the system returns to its initial equilibrium state [35].

Fig. 2a shows the measured optical absorption spectra of the *n-p* and *n-n* homojunction ZnO NW arrays in the wavelength range of 380–800 nm. The peak absorption wavelength is observed at

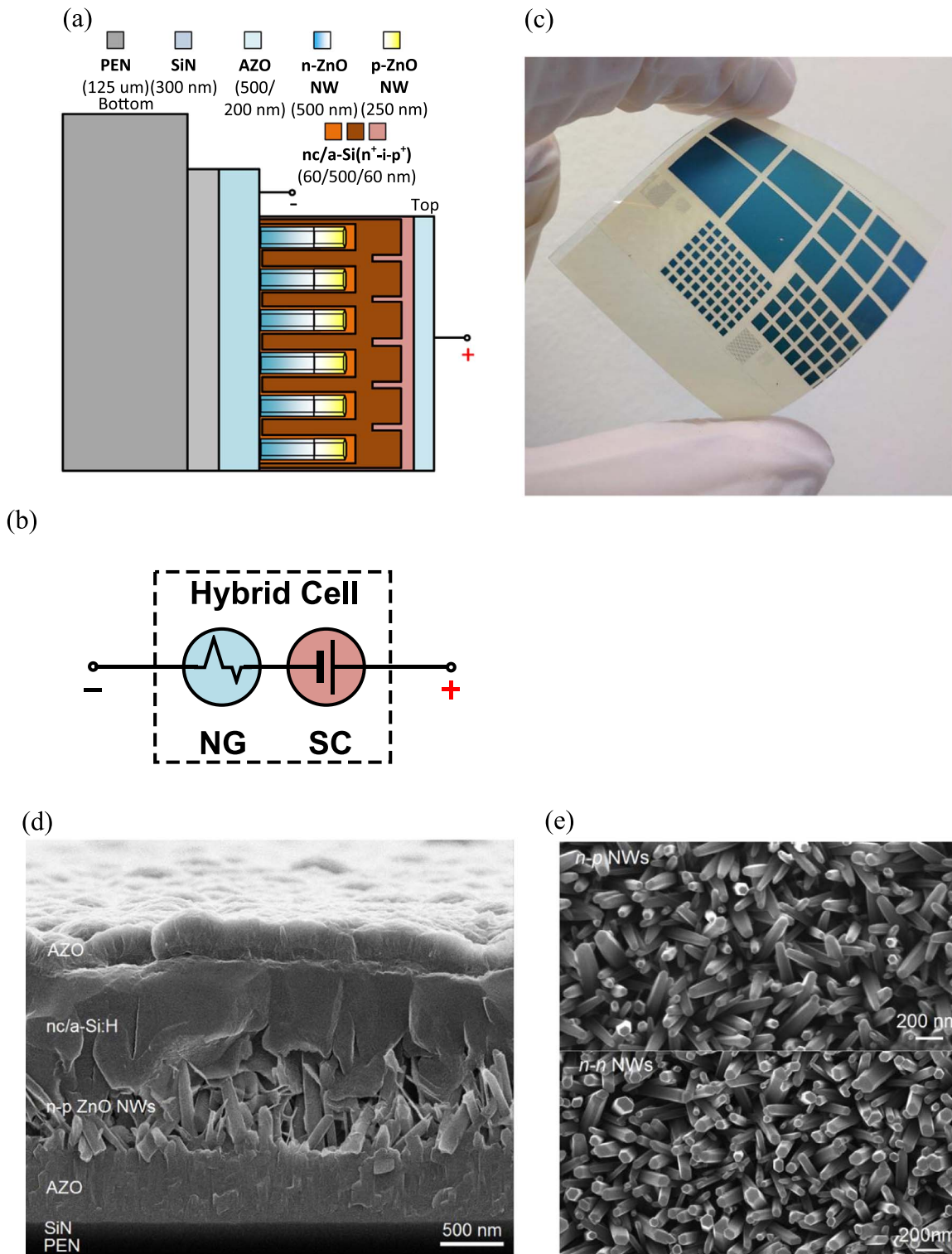


Fig. 1. (a) A schematic diagram of a CHEC made of *n-p* homojunction ZnO NWs grown on a flexible substrate (cross sectional view). (b) A schematic showing an equivalent circuit of the hybrid energy cell. (c) A photograph of patterned CHEC arrays. (d) A cross-sectional helium ion microscopy (HIM) image of a fabricated CHEC. (e) HIM images of the *n-p* (top) and *n-n* (bottom) homojunction ZnO NW arrays.

$\lambda = \sim 385$ nm in the *n-n* homojunction ZnO NWs, corresponding to a bandgap energy of ~ 3.2 eV. This absorption feature can be attributed to the interband optical transition near the conduction/valence band edges of ZnO. The peak absorption in the *n-p* homojunction NWs exhibits a slight red shift to a longer wavelength of ~ 390 nm. The *n-p* homojunction ZnO NWs also show stronger optical absorption over the visible and near-infrared

wavelength range compared with the *n-n* homojunction ZnO NW arrays. The shift in peak wavelength and stronger optical absorption of *n-p* type CHECs enhance photocurrent generation and may improve solar photon harvesting. A few absorption strength oscillations can be observed in the wavelength range between 600 and 800 nm, and can be attributed to the Fabry-Perot resonance along the layer growth direction.

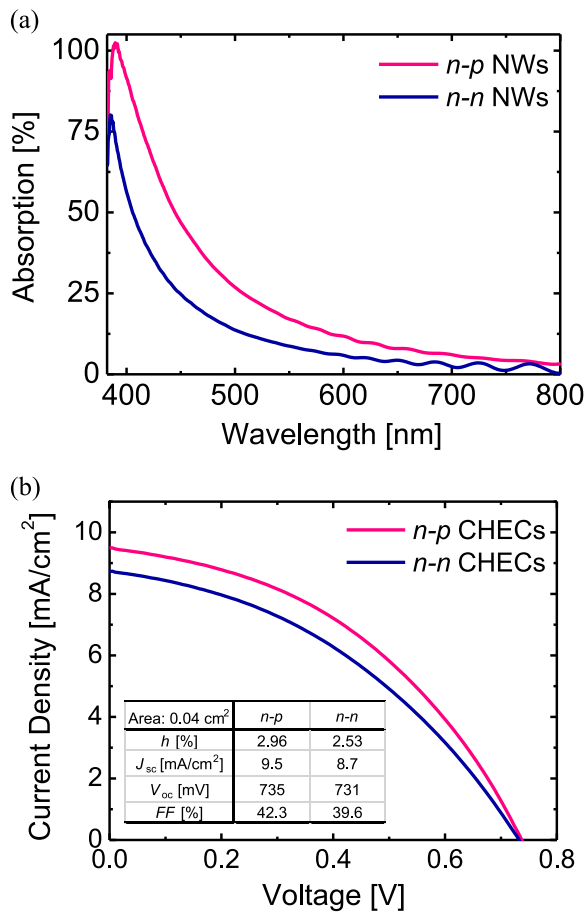


Fig. 2. The measured (a) optical absorption spectra for the *n-p* and *n-n* ZnO homojunction NWs and (b) current density-voltage (*J-V*) characteristics of 2 mm *n-p* and *n-n* CHECs under AM 1.5G illumination with 100 mW/cm² light intensity.

Fig. 2b shows the current density-voltage (*J-V*) curves of the 2 mm-sized *n-n* and *n-p* CHECs under AM 1.5G illumination with 100 mW/cm² light intensity and no mechanical strain. The *n-n* CHECs produce a short-circuit current density (*J*_{sc}) of 8.7 mA/cm², an open-circuit voltage (*V*_{oc}) of 0.731 V, a cell fill factor (*FF*) of 39.6%, and a power conversion efficiency (η) of 2.53%. The CHECs with *n-p* homojunction NWs achieve a higher current density (*J*_{sc}) of 9.5 mA/cm² and efficiency (η) of 2.96%, but similar voltage (*V*_{oc}) of 0.735 V and *FF* of 42.3%. The devices' low solar power conversion efficiency (PCE) is attributed to the roughness of the surfaces and interfaces among the solar cell layers due to their deposition on top of ZnO NWs, roughness further exacerbated by a soft substrate. The marginal improvement in the output current and efficiency of the *n-p* CHECs over those of the *n-n* CHECs might be attributable to the marginally superior optical absorption and the lower internal impedance of *n-p* homojunction NWs.

Larger 1 cm-sized CHECs were used to harvest more solar and mechanical energies. **Fig. S1a** shows a typical current-voltage (*I-V*) curve under dark conditions and no mechanical strain, with an inset of a corresponding semilog *I-V* plot. Almost zero current passes through the CHECs until the voltage exceeds a threshold voltage. A rectifying characteristic is clearly exhibited, demonstrating that the *n-p* and *n-n* homojunction NWs and *n⁺-i-p⁺* Si thin film behave as well-defined diodes. The rectification ratio of the *n-p* CHECs is 1.32×10^4 at bias voltages of -1 and $+1$ V. The turn-on voltage is approximately 0.7 V for both types of CHECs.

The capacitance-voltage responses were measured (**Fig. S2b**) to further reveal the electrical properties of the CHECs. The AC signal was set to 10 mV at 5 kHz, while the DC bias was varied from -1 V

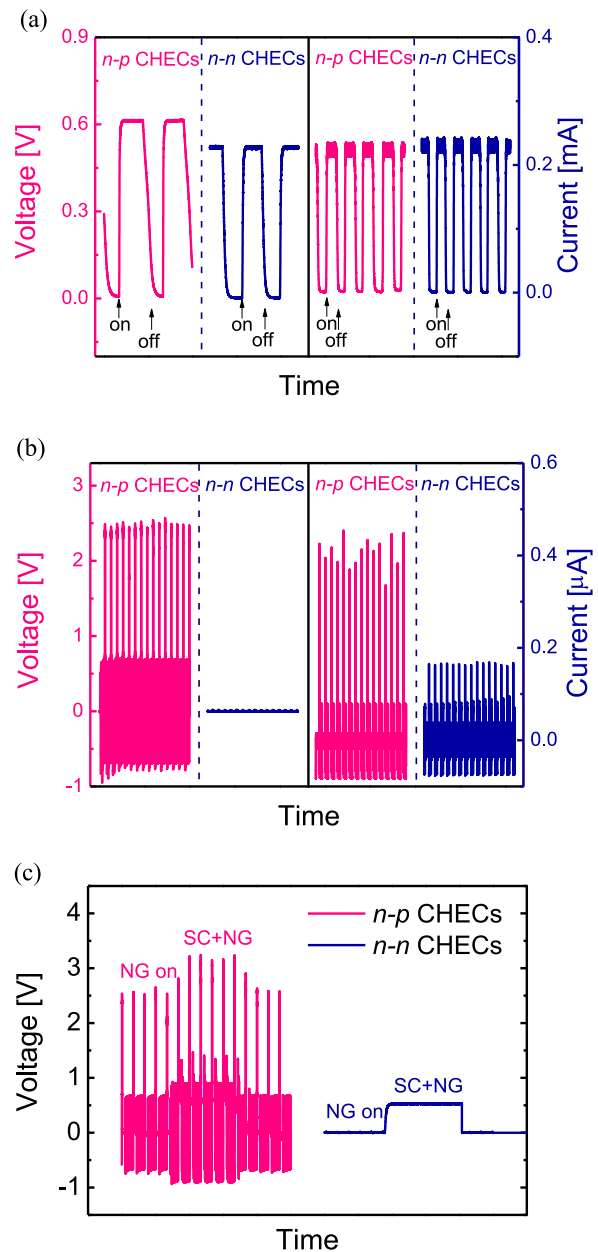


Fig. 3. The open-circuit voltage and short-circuit current of *n-p* and *n-n* CHECs at (a) ambient indoor optical illumination level (~ 10 mW/cm²) and no mechanical strain and (b) an acceleration amplitude of 3 m/s² and a frequency of 3 Hz under dark conditions. (c) The output voltage of the CHECs for combined harvesting of ambient indoor optical illumination of ~ 10 mW/cm² and an acceleration amplitude and frequency of 3 m/s² and 3 Hz, respectively.

to $+3$ V. The anode was connected to the top AZO layer and the cathode to the bottom AZO layer. The results show that capacitance saturates at a larger value for a negative bias voltage (~ 12 nF for *n-p* CHECs, ~ 15 nF for *n-n* CHECs) and at a much smaller value for bias voltages (~ 0.4 nF for both CHECs) in the range of 1–3 V. The measured capacitance exhibits a sharp drop as the DC bias increases from 0 to $+1$ V. The *n-p* CHECs have lower capacitance than the *n-n* CHECs because of the additional junction capacitance associated with the *n-p* ZnO homojunction connected in series with the interface capacitance of *p-ZnO* NW/*n⁺-nc-Si* and the junction capacitance of *n⁺-i-p⁺* Si, resulting in a smaller overall CHEC capacitance.

Fig. 3a shows the voltage output of the 1 cm-sized CHECs under indoor ambient optical illumination (~ 10 mW/cm²) and no

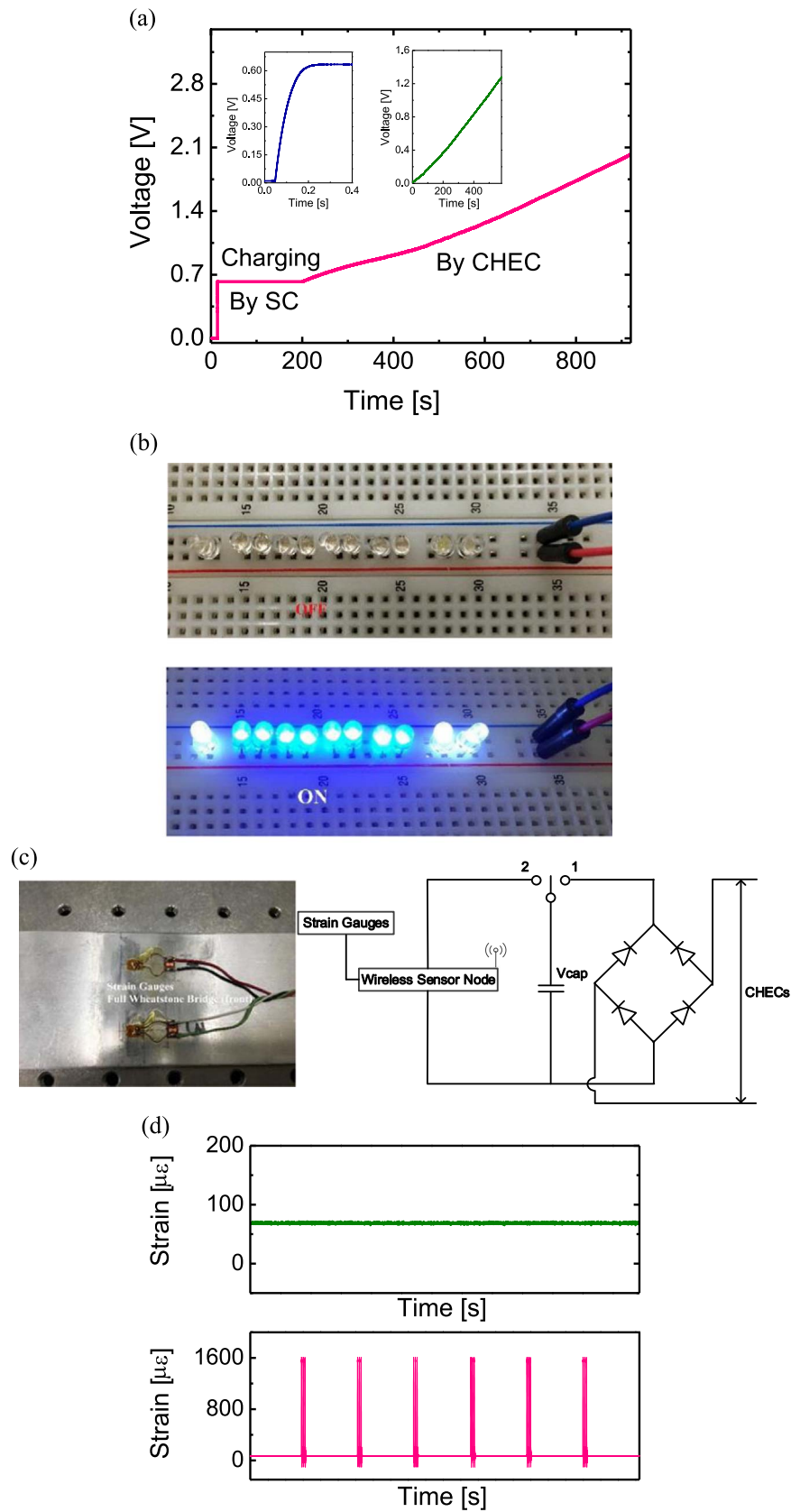


Fig. 4. (a) The charging curves of a $10 \mu\text{F}$ capacitor being charged by an $n-p$ individual CHEC. The insets are the curves for the NG and SC components, separately. (b) A photograph of eight blue and three white LEDs before and after being powered by a charged $1000 \mu\text{F}$ capacitor. (c) A photograph of two commercial strain gauges (the front-side of a Wheatstone bridge) incorporated into the wireless sensor node. (d) The measured strain signals (top) without vibration and (bottom) with vibration from the wireless strain gauge sensor.

mechanical strain. DC-type photovoltaic output was obtained by repeatedly turning the indoor light source on and off at 2 s and 1 s intervals. The *n-p* CHECs yield a higher open-circuit voltage (~ 0.6 V) than the *n-n* CHECs (~ 0.55 V), but comparable current output (~ 280 μ A). From Fig. S1a, the resistance of the *n-p* CHECs is derived to be 1.7 k Ω at 1 V, lower than the resistance (4.5 k Ω) of the *n-n* CHECs. The overall impedance obtained from combining these resistances with the measured capacitance are (1.67 k Ω) for *n-p* type CHECs and (4.27 k Ω) for *n-n* CHECs.

The piezoelectric response of the CHECs under dark conditions is measured and presented in Fig. 3b. The CHECs were anchored on a fixed stopper, and the shaker moved back and forth, applying periodic strain to the NWs by striking the CHECs at the end of each cycle [34,36]. The excitation frequency was set to 3 Hz, and the acceleration amplitude to 3 m/s². AC-type piezoelectric output – positive and negative current passing through the external load – can be observed as the *n-p* homojunction-based NGs (PNGs) undergo cyclic mechanical strain, similar to results reported elsewhere [35,37–39]. In this CHEC, the AC signal is produced from the PNG part, while a positive DC signal is observed from the SC under light illumination. The results show that the open-circuit voltage V_{oc} of the *n-p* CHECs is 138 times higher than that of the *n-n* CHECs, reaching a maximum of +2.5 V, and the maximum short-circuit current I_{sc} is more than twice that of the *n-n* CHECs. The improved V_{oc} and I_{sc} can be attributed to the substantial reduction in mobile charge screening effect observed in the *n-p* homojunction. [34,40].

Although the solar cell (SC) component of the CHECs produces a relatively higher output current – on the order of mA – its output voltage is only around 0.5–0.6 V. Conversely, the output voltage of the PNG can be as high as several volts, but its output current is less than 1 μ A. Hence, a hybridization of the SC and NG could exploit both of their advantages, yielding a higher output current and higher output voltage device. To demonstrate simultaneous harvesting of solar and mechanical energies, the CHECs were tested under indoor optical illumination and mechanical strain. The measured open-circuit voltage is shown in Fig. 3c. During the experiment, an acceleration amplitude of 3 m/s² at 3 Hz frequency was applied continuously. An indoor illumination of ~ 10 mW/cm² was applied for a short period (2 s), and then dark conditions were resumed. For the *n-p* CHECs, the maximum output voltage exceeds 3 V under both optical and mechanical excitation. The results show that the voltage outputs from the SC component and the NG component combine constructively, verifying that the CHEC can simultaneously and individually harvest solar and mechanical energies. The add-on effect is negligible (the right curve in Fig. 3c) in the *n-n* CHECs because the piezoelectric voltage output is quite small.

The hybrid energy cell's potential to charge capacitors, power LEDs, and drive wireless sensor nodes is illustrated using the *n-p* CHECs under ~ 10 mW/cm² illumination and an acceleration amplitude of 3 m/s² at 3 Hz frequency. Their pulsed voltage output is rectified using a full-wave bridge. Fig. 4a shows the charging curves of a 10 μ F capacitor charged by a 1 cm-sized CHEC. Under optical illumination only, the capacitor can be charged from 0 V to 0.61 V in less than 0.3 s. Voltage remains constant afterwards (left inset, Fig. 4a). Under mechanical excitation only, the voltage across the capacitor increases slowly and almost linearly, reaching ~ 1.27 V in 580 s (right inset, Fig. 4a). Under combined optical and mechanical input, the CHEC charges the same capacitor to a voltage of 2.0 V in 920 s. Comparison indicates that the hybrid cell can effectively compensate for the lower voltage output of the solar cell component.

To enhance the CHEC's output, six cells were integrated in series to charge a 1000 μ F capacitor. The capacitor was then deployed to power eight blue and three white LEDs connected in

parallel. The emitted light lasted for 0.5–1.0 s and is clearly captured against the background, in Fig. 4b.

The CHECs' capacity to sustainably drive a wireless sensor node was tested on a commercial EH-LINK wireless sensor (strain gauge) node (LORD Corporation). On this node, the output of six CHECs connected in series was first rectified by the full-wave bridge. The charge was stored in the 1000 μ F capacitor. A custom-made full Wheatstone bridge was implemented using four 350 Ω commercial strain gauge sensors (Vishay precision group) (Fig. 4c) to measure the strain at the instrumented root of a cantilever beam. The wireless strain sensor node was used to transmit the measured strain signal to a USB base station connected to a computer that acquired and recorded data. Fig. 4d shows the recorded strain signals obtained from this experimental setup. The strain in the beam was measured by the wireless sensor node powered by an electronic circuit consisting of the CHECs, the capacitor, and the full-wave bridge. Depending on whether the beam was under mechanical excitation or not, measurable strain signals were recorded (lower graph) or not (upper graph, Fig. 4d). When the excitation frequency of the beam was set to 3 Hz and the acceleration amplitude to 3 m/s², the intermittently-measured strain was about 1600 $\mu\epsilon$. These results demonstrate that the CHECs are capable of powering commercial electronics.

4. Conclusion

This paper presents a compact hybrid energy cell (CHEC) made of an inorganic solar cell monolithically integrated with a ZnO piezoelectric nanogenerator. The nanogenerator is made of vertically aligned *n-p* homojunction ZnO NWs hydrothermally grown on a flexible substrate. The solar cell is made of $n^+ - i - p^+ nc/a\text{-Si:H}$ thin-films. The fabricated CHECs are demonstrated to harvest strain and solar energies individually and concurrently. Employing *n-p* junction based ZnO nanowires in the nanogenerator component improves the piezoelectric voltage output of the CHECs by more than two orders of magnitude (138 times). Under indoor ambient illumination and mechanical excitation with an acceleration of 3 m/s² at 3 Hz frequency, the output current and voltage from a single 1.0 cm-sized *n-p* junction-based CHEC were 280 μ A and 3.0 V, respectively, enough to drive low-power commercial electronics. Six such CHECs connected in series to charge a capacitor harnessed enough energy to light up 8 blue and 3 white LEDs in pulsed mode or to drive a wireless strain gauge sensor node intermittently. This cascade-type ZnO *n-p* homojunction NW CHEC represents a significant step toward effective combined energy harvesting from the ambient environment, offering a flexible power supply for self-powered electronics.

Acknowledgements

This research was supported by Natural Science and Engineering Research Council (NSERC) of Canada, Canadian Foundation of Innovation (CFI), the CMC Microsystems, Ontario Research Fund (ORF), and Ontario Centres of Excellence (OCE). The authors extend their thanks to Bright Iheanacho, Alireza Khosropour, Ruifeng Yang, and Minoli Pathirane for their valuable discussion and technical support.

Appendix A. Supplementary material

Supplementary data associated with this article can be found in the online version at <http://dx.doi.org/10.1016/j.nanoen.2016.06.018>.

References

- [1] M. Law, L.E. Greene, J.C. Johnson, R. Saykally, P. Yang, *Nat. Mater.* 4 (2005) 455.
- [2] C.M. Hsu, C. Battaglia, C. Pahud, Z. Ruan, F.J. Haug, S. Fan, C. Ballif, Y. Cui, *Adv. Energy Mater.* 2 (2012) 628.
- [3] J. Jean, S. Chang, P.R. Brown, J.J. Cheng, P.H. Rekemeyer, M.G. Bawendi, S. Gradečak, V. Bulović, *Adv. Mater.* 25 (2013) 2790.
- [4] W.U. Huynh, J.J. Dittmer, A.P. Alivisatos, *Science* 295 (2002) 2425.
- [5] L. Li, S. Chen, X. Wang, Y. Bando, D. Golberg, *Energy Environ. Sci.* 5 (2012) 6040.
- [6] S. Xu, B.J. Hansen, Z.L. Wang, *Nat. Commun.* 1 (2010) 93.
- [7] Y. Hu, Y. Zhang, C. Xu, L. Lin, R.L. Snyder, Z.L. Wang, *Nano Lett.* 11 (2011) 2572.
- [8] J. Chen, G. Zhu, J. Yang, Q. Jing, P. Bai, W. Yang, X. Qi, Y. Su, Z.L. Wang, *ACS Nano* 9 (2015) 105.
- [9] Z.L. Wang, *Adv. Mater.* 24 (2012) 280.
- [10] C. Xu, Z.L. Wang, *Adv. Mater.* 23 (2011) 873.
- [11] D. Choi, K.Y. Lee, M.-J. Jin, S.-G. Ihn, S. Yun, X. Bulliard, W. Choi, S.Y. Lee, S.-W. Kim, J.-Y. Choi, *Energy Environ. Sci.* 4 (2011) 4607.
- [12] C. Xu, X. Wang, Z.L. Wang, *J. Am. Chem. Soc.* 131 (2009) 5866.
- [13] Y. Yang, H. Zhang, G. Zhu, S. Lee, Z.-H. Lin, Z.L. Wang, *ACS Nano* 7 (2012) 785.
- [14] C. Pan, W. Guo, L. Dong, G. Zhu, Z.L. Wang, *Adv. Mater.* 24 (2012) 3356.
- [15] G.C. Yoon, K.-S. Shin, M.K. Gupta, K.Y. Lee, J.-H. Lee, Z.L. Wang, S.-W. Kim, *Nano Energy* 12 (2015) 547.
- [16] Y. Zi, L. Lin, J. Wang, S. Wang, J. Chen, X. Fan, P.K. Yang, F. Yi, Z.L. Wang, *Adv. Mater.* 27 (2015) 2340.
- [17] J.H. Lee, K.Y. Lee, M.K. Gupta, T.Y. Kim, D.Y. Lee, J. Oh, C. Ryu, W.J. Yoo, C.Y. Kang, S.J. Yoon, *Adv. Mater.* 26 (2014) 765.
- [18] L. Zheng, G. Cheng, J. Chen, L. Lin, J. Wang, Y. Liu, H. Li, Z.L. Wang, *Adv. Energy Mater.* (2015).
- [19] Y. Yang, H. Zhang, J. Chen, S. Lee, T.-C. Hou, Z.L. Wang, *Energy Environ. Sci.* 6 (2013) 1744.
- [20] Y. Yang, H. Zhang, Y. Liu, Z.-H. Lin, S. Lee, Z. Lin, C.P. Wong, Z.L. Wang, *ACS Nano* 7 (2013) 2808.
- [21] Y. Yang, H. Zhang, S. Lee, D. Kim, W. Hwang, Z.L. Wang, *Nano Lett.* 13 (2013) 803.
- [22] Y. Hu, J. Yang, S. Niu, W. Wu, Z.L. Wang, *ACS Nano* 8 (2014) 7442.
- [23] G. Cheng, Z.-H. Lin, Z.-I. Du, Z.L. Wang, *ACS Nano* 8 (2014) 1932.
- [24] X. Wang, S. Wang, Y. Yang, Z.L. Wang, *ACS Nano* 9 (2015) 4553.
- [25] Y. Yang, H. Zhang, Z.-H. Lin, Y. Liu, J. Chen, Z. Lin, Y.S. Zhou, C.P. Wong, Z. L. Wang, *Energy Environ. Sci.* 6 (2013) 2429.
- [26] B.J. Hansen, Y. Liu, R. Yang, Z.L. Wang, *ACS Nano* 4 (2010) 3647.
- [27] R. Yang, Y. Qin, C. Li, G. Zhu, Z.L. Wang, *Nano Lett.* 9 (2009) 1201.
- [28] S. Lee, S.-H. Bae, L. Lin, S. Ahn, C. Park, S.-W. Kim, S.N. Cha, Y.J. Park, Z.L. Wang, *Nano Energy* 2 (2013) 817.
- [29] C. Xu, C. Pan, Y. Liu, Z.L. Wang, *Nano Energy* 1 (2012) 259.
- [30] C. Pan, S. Niu, Y. Ding, L. Dong, R. Yu, Y. Liu, G. Zhu, Z.L. Wang, *Nano Lett.* 12 (2012) 3302.
- [31] Z. Wang, R. Yu, X. Wen, Y. Liu, C. Pan, W. Wu, Z.L. Wang, *ACS Nano* 8 (2014) 12866.
- [32] J.C. Shin, P.K. Mohseni, K.J. Yu, S. Tomasulo, K.H. Montgomery, M.L. Lee, J. A. Rogers, X. Li, *ACS Nano* 6 (2012) 11074.
- [33] L.E. Greene, M. Law, J. Goldberger, F. Kim, J.C. Johnson, Y. Zhang, R.J. Saykally, P. Yang, *Angew. Chem. Int. Ed.* 42 (2003) 3031.
- [34] G. Liu, E. Abdel-Rahman, D. Ban, *J. Appl. Phys.* 118 (2015) 094307.
- [35] K.Y. Lee, B. Kumar, J.-S. Seo, K.-H. Kim, J.I. Sohn, S.N. Cha, D. Choi, Z.L. Wang, S.-W. Kim, *Nano Lett.* 12 (2012) 1959.
- [36] L. Lin, Q. Jing, Y. Zhang, Y. Hu, S. Wang, Y. Bando, R.P. Han, Z.L. Wang, *Energy Environ. Sci.* 6 (2013) 1164.
- [37] J. Briscoe, M. Stewart, M. Vopson, M. Cain, P.M. Weaver, S. Dunn, *Adv. Energy Mater.* 2 (2012) 1261.
- [38] K. Pradel, W. Wu, Y. Ding, Z.L. Wang, *Nano Lett.* (2014).
- [39] Y.H. Kwon, D.-H. Kim, H.-K. Kim, J. Nah, *Nano Energy* 18 (2015) 126.
- [40] K.C. Pradel, W. Wu, Y. Ding, Z.L. Wang, *Nano Lett.* 14 (2014) 6897.



Guocheng Liu received his Ph.D. in Electrical and Computer Engineering from University of Waterloo, Canada. He is currently a Postdoctoral Fellow at University of Waterloo. His research mainly focuses on the integration of two-dimensional nanostructured material for semiconductor and optoelectronic devices, including device design, modelling, fabrication, characterization, and applications.



Nezih Mrad received the Ph.D. degree in engineering from Pennsylvania State University at University Park in 1995. He is head of the office of chief scientist (ADM (S&T)) at Defence R&D Canada (DRDC) the Department of National Defence, Canada. He served as an adjunct professor and lecturer at several Canadian universities, such as Carleton University, Concordia University, the University of Sherbrooke, and as a professor at Penn State University and the University of South Carolina. He has extensive experience in defence, safety and security related emerging technologies including advanced sensing, wireless sensor networks, energy harvesting, and novel materials systems. He conducted and managed R&D activities in CBM, SHM, PHM, micro and nanotechnologies, as they relate to platform life cycle cost reduction, improved performance, increased safety and enhanced logistics support. He has authored and/or coauthored over 250 publications, including books and book chapters. Dr. Mrad serves on the editorial board of several journals, including the Canadian Military Journal, and led the development of several journals' special issues. He chaired and co-chaired a number of national, international committees, conferences, and workshops on issues ranging from novel sensors and energy harvesting to advanced propulsion systems.



Eihab Abdel-Rahman is an Associate Professor of System Design Engineering at University of Waterloo. His research interests are in the electromechanical systems and nonlinear dynamics of MEMS, electrostatic and electromagnetic actuators and sensors, and energy harvesters. His research has resulted in the discovery of new phenomena in micro-systems, the development of innovative MEMS sensors and actuators, and novel micro power generators. He has co-authored more than 150 refereed journal and conference papers and filed seven patents on sensors and energy harvesters.



Dayan Ban is a Professor of Nanotechnology Engineering in the Department of Electrical and Computer Engineering of the University of Waterloo. He received a B.Sc. and M.A.Sc at the University of Science and Technology of China, Hefei, China. He received a Ph.D. in Electrical and Computer Engineering from the University of Toronto, Toronto, Ontario, Canada, in 2003. During 2001–2002, he was a visiting scientist at Nortel Networks Optical Components, Ottawa, Ontario, Canada. Dr. Ban was on staff at the Institute for Microstructural Sciences of the National Research Council, Ottawa, from Sept. 2002 to Oct. 2005. He was a visiting scientist with the Research Lab of Electronics at MIT in 2009. Dr. Ban is a senior member of IEEE/LEOS and a registered Professional Engineer in Ontario. He has over 15 years experience in designing, fabricating, characterizing optoelectronic devices as well as in scanning probe microscopy technique. Dr. Ban has authored or coauthored over 140 papers in refereed journals and conference proceedings and has contributed a chapter to the seminal book on novel scanning probe microscopy. He holds four patents in novel optoelectronic devices. His research group has demonstrated several records, including the highest lasing temperature of Terahertz quantum cascade lasers (199.5 K) and the first optical upconversion amplifier.